Channel Estimation and Synchronization Techniques for UWB Communications

Master Thesis

By

Apollon Maniadakis

Submitted to the Department of Electronic & Computer Engineering

in partial fulfillment of the requirements for the Master Degree.

Technical University of Crete

Associate Professor Liavas Athanasios (Supervisor)

Professor Sidiropoulos Nikolaos

Associate Professor Potamianos Alexandros

January 2007

Contents

List of Figures

Chapter 1

INTRODUCTION

1.1 UWB Definition

Ultra-wideband (UWB) radio is a fast emerging technology with uniquely attractive features inviting major advances in wireless communications, networking, radar, imaging, and positioning systems. By its rule-making proposal in 2002, the Federal Communications Commission (FCC) essentially unleashed huge 'new bandwidth' (3.6 - 10.1 GHz) at the noise floor, where UWB radios overlaying coexistent RF systems can operate using low-power ultra-short information bearing pulses [1]. Ultra wideband (UWB) communications systems can be broadly clas-

sified as any communication system whose instantaneous bandwidth is many times greater than the minimum required to deliver particular information. This excess bandwidth is the defining characteristic of UWB. Thus, UWB technology offers a promising solution to the RF spectrum drought by allowing new services to coexist with current radio systems with minimal or no interference [2]. Figure 1.1 shows the coexistence between narrowband, wideband and UWB systems.

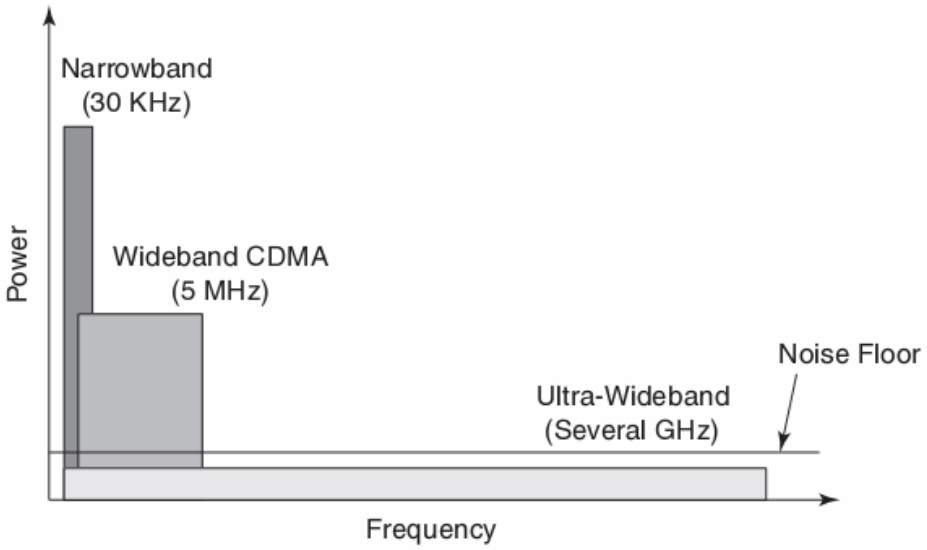

Figure 1.1: Coexistence of UWB signals with narrowband and wideband signals in the RF spectrum

1.2 UWB Concepts

What makes UWB systems unique is their large instantaneous bandwidth and the ability to provide high data rate at low cost and low power consumption. Additionally, the wide bandwidth and potential for low-cost digital design enable a single system to operate in different modes as a communications device, radar, or locator. Taken together, these properties give UWB systems a clear technical advantage over other more conventional approaches in high multipath environments at low to medium data rates.

UWB systems use carrierless, short-duration (picosecond to nanosecond) pulses for transmission and reception of the information. Since frequency is inversely related to time, the short-duration UWB pulses spread their energy across a wide range of frequencies — from near DC to several gigahertz (GHz) — with very low power spectral density (PSD) [3].

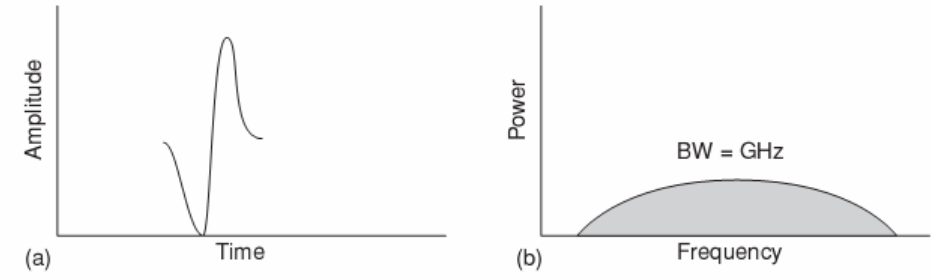

Figure 1.2: A UWB pulse in (a) the time and (b) the frequency domain.

Figure 1.2 illustrates UWB pulses in time and frequency domains. The wide instantaneous bandwidth results from the time-scaling property of theoretical Fourier transforms:

$$x(at) \longleftrightarrow \frac{1}{|a|} X\left(\frac{f}{a}\right) \tag{1}$$

The notation on the left side of Equation (1) shows a signal, $x(t)$, which is scaled in the time domain by a factor a; the right side represents the same signal in the frequency domain, $X(f)$, which is inversely scaled by the same factor a and its bandwidth is expanded a times. The UWB bandwidth is the frequency band bounded by the points that are 10 dB below the highest radiated emission, as based on the complete transmission system including the antenna. The upper boundary is designated f_h and the lower boundary is designated f_l. The center

frequency ,f_c, equals $(f_h + f_l)/2$ [4].

For example, a pulse with duration T of 500 picoseconds can generate a center frequency f_c of 2 GHz (Figure 1.3):

$$f_c = \frac{1}{T} = \frac{1}{500 \times 10^{-12}} = 2 \times 10^9 Hz = 2GHz$$

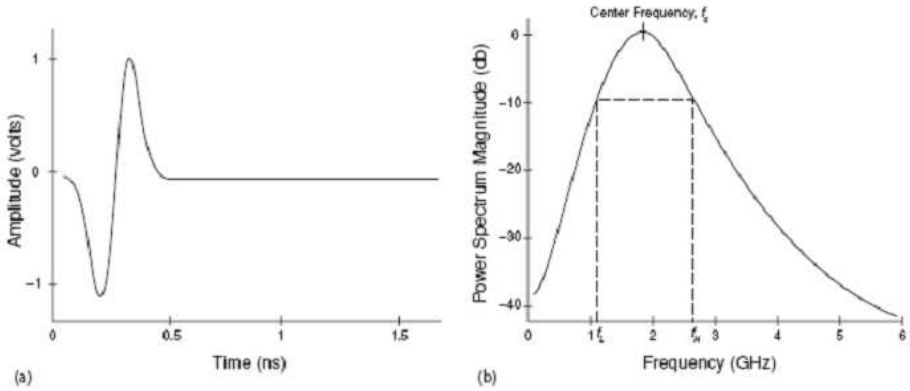

Figure 1.3: A 500-picosecond Gaussian monocycle in (a) the time and (b) the frequency domain.

1.3 UWB Signals

There are two common forms of UWB: one based on sending very short duration pulses to convey information (Impulse UWB, I-UWB) and another approach using multiple simultaneous carriers (Multicarrier UWB, MC-UWB). In this thesis, we concentrate on I-UWB [2].

As defined by the FCC, UWB signals must have bandwidths greater than 500 MHz or a fractional bandwidth larger than 20 percent at all times of transmission [4]. Fractional bandwidth is a factor used to classify signals as narrowband, wideband, or ultra-wideband and is defined by the ratio of bandwidth at -10 dB points[1] to center frequency. Equation (2) shows this relationship:

$$B_f = \frac{BW}{f_c} \times 100\% = \frac{(f_h - f_l)}{(f_h + f_l)/2} \times 100\% = \frac{2(f_h - f_l)}{f_h + f_l} \times 100\% \qquad (2)$$

where f_h and f_l are the highest and lowest cutoff frequencies (at the -10 dB point) of a UWB pulse spectrum respectively and BW is the absolute bandwidth.

[1]The -10 dB point represents the spectral power of a signal at 10 dB lower than its peak power (as mentioned before).

A UWB signal can be any one of a variety of wideband signals, such as Gaussian, chirp, wavelet, or Hermite-based short-duration pulses. UWB systems also allow for several modulation schemes, including Pulse Position Modulation(PPM), Pulse Amplitude Modulation (PAM), On-Off Keying (OOK) and Binary Phase Shift Keying (BPSK) (Figure 1.4).

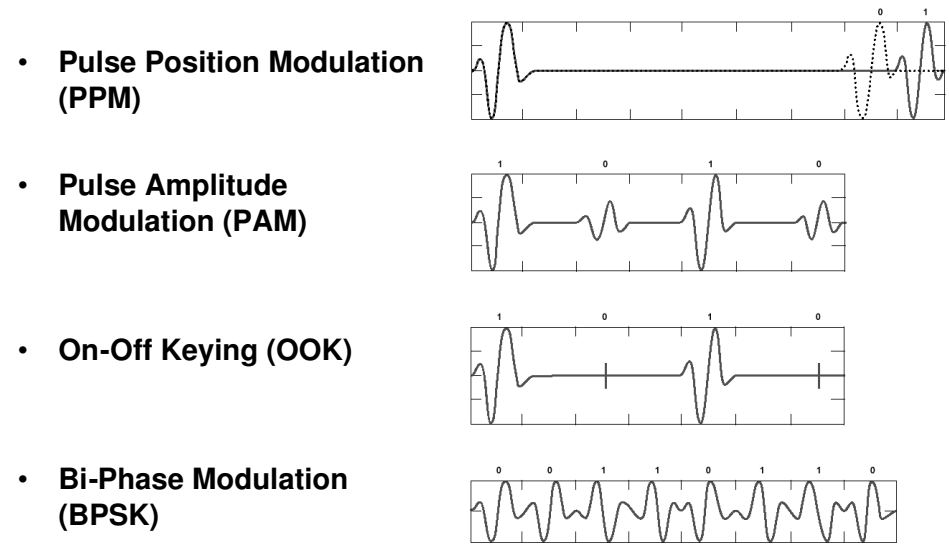

Figure 1.4: Modulation schemes of UWB signals

1.4 Advantages of UWB Technology

The nature of the short-duration pulses used in UWB technology offers several advantages over narrowband communications systems. Here, we name a few [5]:

1. Accurate position location and ranging, due to the fine time resolution
2. No significant multipath fading due to fine time resolution
3. Multiple access due to wide transmission bandwidths
4. Possibility of high data rates
5. Covert communications due to low transmission power operation
6. Possible easier material penetration due to the presence of energy at different frequencies

1.5 Applications and Environments of Interest

An important application are personal area networks (PANs), where data are transmitted over distances of 10 m or less. Among the PANs, we can distinguish between high data rate (100 Mbit/s and up) mainly related to consumer electronics and computer networks and low data rate applications including Bluetooth and infrared devices. Irrespective of those data rate considerations, the envisioned environments are mainly office and residential structures, with distances between 1 and 10 m.

Another emerging application are sensor networks. As the data rate is much lower (typically 1 kbit/s-1 Mbit/s), the possible range is considerably larger, namely up to about 100-300 m. Applications include monitoring of residential and office environments, plant monitoring, security monitoring at airports and convention centers, as well as outdoor monitoring. Therefore, office environments with large distances between transmitter and receiver, factory halls, airport halls and outdoor scenarios are all environments of interest. Again, the frequency

range 3.1 - 10.6 GHz is most relevant.

The large bandwidth of UWB systems offers the possibility of high-precision ranging, and therefore geolocation. For this application, the first arriving path of the impulse response plays a crucial role - this is in contrast to traditional channel measurements and modeling, where quantities such as path loss and delay spread are of high interest. This is true irrespective of the frequency that is used for the transmission of the ranging signals.

UWB research and development has to cope with formidable challenges that limit their bit error rate (BER) performance, capacity, throughput, and network flexibility. Those include high sensitivity to synchronizing the reception of ultra-short pulses, optimal exploitation of fading propagation effects with pronounced frequency selectivity, low-complexity constraints in decoding high-performance multiple access protocols and strict power limitations imposed by the desire to minimize interference among UWB communicators and with coexisting legacy systems, particularly GPS, vehicles, aircraft radar and WLANs. These challenges call for advanced digital signal processing

expertise to accomplish tasks such as synchronization, channel estimation and equalization, multiuser detection, high-rate high-precision low-power analog/digital conversion and suppression of aggregate interference arising from coexisting legacy systems [5], [6].

Chapter 2

CHANNEL ESTIMATION FOR UWB SIGNALS

2.1 Introduction

Channel estimation is a core issue for receiver design in wireless communications systems. Because it is not possible to measure every wireless channel in the field, it is important to use training sequences to estimate channel parameters, such as attenuations and delays of the propagation path. Given that most UWB receivers correlate the re-

ceived signal with a predefined template signal, prior knowledge of the wireless channel parameters is necessary to predict the shape of the template signal that matches the received one. However, as a result of the wide bandwidth and reduced signal energy, UWB pulses undergo severe pulse distortion; thus, channel estimation in UWB communications systems becomes very complicated.

2.2 Signal Format and Rake Receiver

In a multipath environment, the exploitation of the channel diversity calls for sophisticated receivers. Multiuser detection is known to be the optimal solution but, as its complexity increases exponentially with the number of users, it is often impractical. Suboptimal schemes are indispensable. In this context, the Rake receiver is a good tradeoff between high-performance and low-complexity.

In a Rake receiver, each signal echo is correlated with a locally generated time-hopping pulse train and then combined into a single test variable for final decision. Time alignment is required between the code sequence in each echo and the corresponding locally generated reference. Also, the attenuations incurred by the various echoes must be known to maximize the signal-to-noise ratio (SNR) in the decision variable (maximal ratio combining). In conclusion, proper Rake operation requires information about the delays and attenuations of the channel paths.

In order to estimate these parameters, we adopt a maximum-likelihood

(ML) approach and consider the scenario with data-aided (DA) estimation [7]. This is of interest during channel *acquisition*, when a training sequence is available. Channel *tracking* can be pursued in a pilot-aided fashion, by periodically retransmitting the training sequence, or in a decision-directed (DD) manner using the receiver decisions in place of true data.

The signal transmitted by the desired user, using PPM modulation, is modeled as [8]

$$s(t) = \sum_i b(t - iNT_f - a_i\Delta) \tag{2.1}$$

where

$$b(t) = \sum_{j=0}^{N-1} g(t - jT_f - c_jT_c) \tag{2.2}$$

In the last equation, $g(t)$ is the basic pulse used to convey information (referred to as *monocycle*) and T_f is the frame time, i.e., the separation between adjacent monocycles when the symbols c_j are identically zero. The ratio of T_f to the duration of the monocycle D_g is the *duty cycle* and may be on the order of a hundred or more. The sequence $\{c_j\}$ is the user's time-hopping code and its elements are integers taking

values in the range $0 \leq c_j \leq N_h - 1$. In our case, we consider the scenario with one single user, so the time-hopping code $c_j = 0$, $j = 0, 1, \ldots, N-1$. Dividing each frame into N_c chips, the parameter T_c is the duration of each chip. The a_i represent the data symbols and are modeled as binary (0 or 1) independent and identically distributed (i.i.d.) random variables. Correspondingly, Δ may be viewed as the time shift impressed by a unit data on the monocycles of a block, as this indicated by the PPM modulation that we use. Finally, N is the number of frames over which a single symbol is spread.

When the signal is transmitted over a channel with L_c paths, the received waveform at the output of the receiver antenna may be written as

$$r(t) = \sum_{l=1}^{L_c} \gamma_l s(t - \tau_l) + w(t) \tag{2.3}$$

In this equation, $s(t)$ is the desired user's signal, γ_l and τ_l are the attenuation and the delay affecting its replica travelling through the lth path and $w(t)$ is white Gaussian noise. In writing (2.3), we have implicitly assumed a static channel, meaning that γ_l and τ_l are either

fixed or vary so slowly that they are practically constant over several data symbols.

A simple, suboptimal detection process is achieved by computing the correlation

$$y_k^{(1)} = \int_{kNT_f}^{(k+1)NT_f} r(t)\nu(t - kNT_f - \tau_1)dt$$

with $\nu(t) = b(t) - b(t - \Delta)$ and deciding that a_k equals either zero or one according to whether $y_k^{(1)}$ is greater or less than zero [7]. As is clear from (2.2), the template signal $\nu(t)$ depends not only on the user's time-hopping code, but also on $g(t)$. For purpose of analysis, we assume that the shape of the monocycle is known.

The above detector may be viewed as a Rake receiver with a single finger (Rake - 1). Note that, although Rake - 1 needs to know the strongest path and the associated delay, it does not care about the actual value of the path gain.

A better result is obtained by exploiting L signal echoes rather than just one. This leads to a Rake receiver with L fingers (Rake - L), whose block diagram is depicted in Fig. 2.1.

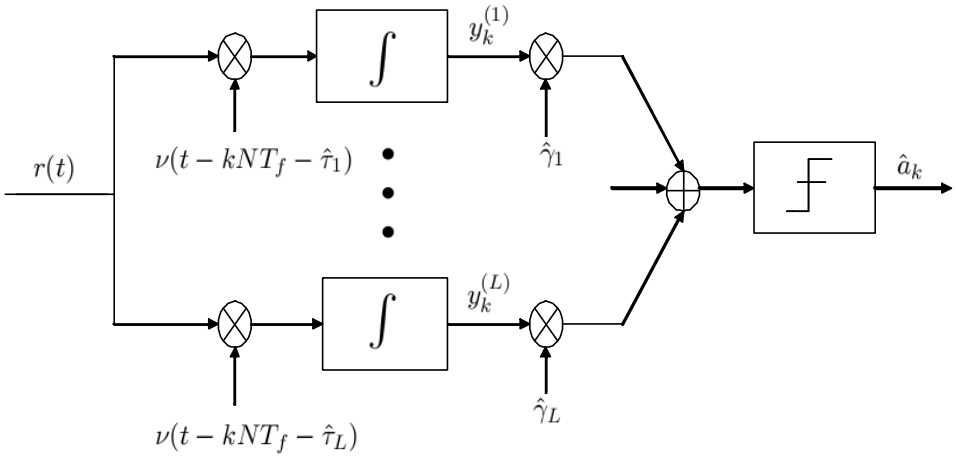

Figure 2.1: Block diagram of a Rake-L receiver

The decision statistic is now the *maximal-ratio* combination of the correlators' outputs [7]

$$z_k = \sum_{l=1}^{L} \gamma_l \int_{kNT_f}^{(k+1)NT_f} r(t)\nu(t - kNT_f - \tau_l)dt.$$

In practice, the parameters $\{\gamma_l\}$ and $\{\tau_l\}$ are not known *a priori* and must be estimated.

2.3 Data-Aided Technique (ML Estimation)

The received waveform is observed over an interval $0 \leq t \leq T_0$, with T_0 a multiple M of the symbol period NT_f. The noise $w(t)$ has a spectral density $N_0/2$. The parameters $\boldsymbol{\gamma} = (\gamma_1, \gamma_2 \cdots \gamma_{L_c})$ and $\boldsymbol{\tau} = (\tau_1, \tau_2 \cdots \tau_{L_c})$ are viewed as unknown deterministic quantities and, for the time being, the number of paths L_c is taken as a known quantity. We use a notation of the type $\tilde{x}$ to indicate a trial value of a variable x and we define as

$$\tilde{s}(t) = \sum_{l=1}^{L_c} \tilde{\gamma}_l s(t - \tilde{\tau}_l) \tag{2.4}$$

a possible realization of the signal component in (2.4) corresponding to the channel parameters $\tilde{\boldsymbol{\gamma}}$ and $\tilde{\boldsymbol{\tau}}$.

Substituting (2.4) into (2.3), we get

$$r(t) = \tilde{s}(t) + w(t) \tag{2.5}$$

Let $\mathbf{r}$, $\mathbf{s}(\tilde{\boldsymbol{\gamma}}, \tilde{\boldsymbol{\tau}})$ and $\mathbf{w}$ be vector representations of $r(t)$, $\tilde{s}(t)$ and $w(t)$ over a complete orthonormal basis $\{\phi_i(t)\}$ truncated to N components [9]:

$$\mathbf{r} \triangleq (r_1, r_2, \ldots, r_N)$$

$$\mathbf{s}(\tilde{\boldsymbol{\gamma}}, \tilde{\boldsymbol{\tau}}) \stackrel{\Delta}{=} [s_1(\tilde{\boldsymbol{\gamma}}, \tilde{\boldsymbol{\tau}}), s_2(\tilde{\boldsymbol{\gamma}}, \tilde{\boldsymbol{\tau}}), \ldots, s_N(\tilde{\boldsymbol{\gamma}}, \tilde{\boldsymbol{\tau}})]$$

$$\mathbf{w} \stackrel{\Delta}{=} (w_1, w_2, \ldots, w_N)$$

In particular, the k-th component of $\mathbf{r}$, $\mathbf{s}(\tilde{\boldsymbol{\gamma}}, \tilde{\boldsymbol{\tau}})$ and $\mathbf{w}$ is given by

$$\begin{aligned} r_k &\stackrel{\Delta}{=} \int_0^{T_0} r(t)\phi_k(t)dt \\ s_k(\tilde{\boldsymbol{\gamma}}, \tilde{\boldsymbol{\tau}}) &\stackrel{\Delta}{=} \int_0^{T_0} \tilde{s}(t)\phi_k(t)dt \\ w_k &\stackrel{\Delta}{=} \int_0^{T_0} w(t)\phi_k(t)dt \end{aligned}$$

From (2.5), using the above definitions, we get

$$\mathbf{r} = \mathbf{s}(\tilde{\boldsymbol{\gamma}}, \tilde{\boldsymbol{\tau}}) + \mathbf{w} \tag{2.6}$$

Recognizing the independent and Gaussian nature of the noise $\mathbf{w}$ leads to the result

$$\begin{aligned} p(\mathbf{r}|\tilde{\boldsymbol{\gamma}}, \tilde{\boldsymbol{\tau}}) &= \prod_{k=1}^{N} \frac{1}{2\pi N_0} \exp\left\{ - \frac{\left| r_k - s_k(\tilde{\boldsymbol{\gamma}}, \tilde{\boldsymbol{\tau}}) \right|^2}{2N_0} \right\} \\ &= C_n \exp\left\{ - \frac{1}{2N_0} \sum_{k=1}^{N} \left| r_k - s_k(\tilde{\boldsymbol{\gamma}}, \tilde{\boldsymbol{\tau}}) \right|^2 \right\} \end{aligned} \tag{2.7}$$

with

$$C_n = (2\pi N_0)^{-N}$$

If we denote $\tilde{\boldsymbol{\lambda}} = (\tilde{\boldsymbol{\gamma}}, \tilde{\boldsymbol{\tau}})$, our goal is to maximize $p(\mathbf{r}|\tilde{\boldsymbol{\lambda}})$. Then the ML *estimate* of $\tilde{\boldsymbol{\lambda}}$ is given by

$$\hat{\boldsymbol{\lambda}}_{ML}(\mathbf{r}) = \arg\left\{ \max_{\tilde{\boldsymbol{\lambda}}} \{p(\mathbf{r}|\tilde{\boldsymbol{\lambda}})\} \right\} \tag{2.8}$$

The maximum of $p(\mathbf{r}|\tilde{\boldsymbol{\lambda}})$ can be sought by replacing $p(\mathbf{r}|\tilde{\boldsymbol{\lambda}})$ by

$$\Lambda(\mathbf{r}|\tilde{\boldsymbol{\lambda}}) \triangleq \frac{1}{B}\, p(\mathbf{r}|\tilde{\boldsymbol{\lambda}}) \tag{2.9}$$

where B is any positive constant independent of $\tilde{\boldsymbol{\lambda}}$. In particular, if we choose

$$B = C_n \exp\left\{ -\frac{1}{2N_0} \sum_{k=1}^{N} \left| r_k \right|^2 \right\} \tag{2.10}$$

and note that

$$\left| r_k - s_k(\tilde{\boldsymbol{\lambda}}) \right|^2 = \left| r_k \right|^2 + \left| s_k(\tilde{\boldsymbol{\lambda}}) \right|^2 - 2Re\Big\{ r_k s_k^*(\tilde{\boldsymbol{\lambda}}) \Big\} \tag{2.11}$$

equation (2.9) becomes

$$\Lambda(\boldsymbol{r}|\tilde{\boldsymbol{\lambda}}) = \exp\left\{ \frac{1}{N_0} \sum_{k=1}^{N} Re\big\{ r_k s_k^*(\tilde{\boldsymbol{\lambda}}) \big\} - \frac{1}{2N_0} \sum_{k=1}^{N} \left| s_k(\tilde{\boldsymbol{\lambda}}) \right|^2 \right\} \tag{2.12}$$

One important feature of this formula is that the argument of the exponential converges as N tends to infinity [10].

Now, consider the location of the maximum of $\Lambda(\mathbf{r}|\tilde{\boldsymbol{\lambda}})$

$$\hat{\boldsymbol{\lambda}}(\mathbf{r}) = \arg\left\{ \max_{\tilde{\boldsymbol{\lambda}}} \left\{ \Lambda(\mathbf{r}|\tilde{\boldsymbol{\lambda}}) \right\} \right\} \tag{2.13}$$

Clearly, $\hat{\boldsymbol{\lambda}}(\mathbf{r})$ is only an approximation to $\hat{\boldsymbol{\lambda}}_{ML}(\mathbf{r})$ since the function $\Lambda(\mathbf{r}|\tilde{\boldsymbol{\lambda}})$ does not incorporate all the information contained in $r(t)$. The approximation improves, however, when N increases and in fact the limit of $\hat{\boldsymbol{\lambda}}(\mathbf{r})$ as N tends to infinity provides the exact value of $\hat{\boldsymbol{\lambda}}_{ML}(\mathbf{r})$. On the other hand, we have

$$\lim_{N\to\infty} \sum_{k=1}^{N} Re\Big\{ r_k s_k^*(\tilde{\boldsymbol{\lambda}}) \Big\} = \int_0^{T_0} Re\Big\{ r(t)\tilde{s}^*(t,\tilde{\boldsymbol{\lambda}}) \Big\} dt \tag{2.14}$$

$$\lim_{N\to\infty} \sum_{k=1}^{N} \Big| s_k(\tilde{\boldsymbol{\lambda}}) \Big|^2 = \int_0^{T_0} \Big| \tilde{s}(t,\tilde{\boldsymbol{\lambda}}) \Big|^2 dt \tag{2.15}$$

so that the limit of $\Lambda(\mathbf{r}|\tilde{\boldsymbol{\lambda}})$ takes the form

$$\Lambda(\mathbf{r}|\tilde{\boldsymbol{\lambda}}) = \exp\left\{ \frac{1}{N_0} \int_0^{T_0} Re\big\{ r(t)\tilde{s}^*(t,\tilde{\boldsymbol{\lambda}}) \big\} dt - \frac{1}{2N_0} \int_0^{T_0} \Big| \tilde{s}(t,\tilde{\boldsymbol{\lambda}}) \Big|^2 \right\} dt \tag{2.16}$$

In our case, the waveforms are real-valued, so equation (2.16) can be rewritten as

$$\Lambda(\mathbf{r}|\tilde{\boldsymbol{\lambda}}) = \exp\left\{ \frac{2}{N_0} \int_0^{T_0} r(t)\tilde{s}(t,\tilde{\boldsymbol{\lambda}}) dt - \frac{1}{N_0} \int_0^{T_0} \tilde{s}^2(t,\tilde{\boldsymbol{\lambda}}) dt \right\} \tag{2.17}$$

and $\hat{\boldsymbol{\lambda}}_{ML}(\mathbf{r})$ is computed as

$$\hat{\boldsymbol{\lambda}}_{ML}(\mathbf{r}) = \arg\left\{ \max_{\tilde{\boldsymbol{\lambda}}} \{\Lambda(\mathbf{r}|\tilde{\boldsymbol{\lambda}})\} \right\} \tag{2.18}$$

The function $\Lambda(\mathbf{r}|\tilde{\boldsymbol{\lambda}})$ is referred to as the *likelihood function*. Then the log-likelihood function of the pair $\tilde{\boldsymbol{\lambda}} = (\tilde{\boldsymbol{\gamma}}, \tilde{\boldsymbol{\tau}})$ takes the form

$$\log[\Lambda(\tilde{\boldsymbol{\gamma}}, \tilde{\boldsymbol{\tau}})] = 2\int_0^{T_0} r(t)\tilde{s}(t)dt - \int_0^{T_0} \tilde{s}^2(t)dt \tag{2.19}$$

A more convenient expression for $\log[\Lambda(\tilde{\boldsymbol{\gamma}}, \tilde{\boldsymbol{\tau}})]$ is obtained substituting (2.4) into (2.19)

$$\log[\Lambda(\tilde{\boldsymbol{\gamma}}, \tilde{\boldsymbol{\tau}})] = 2\int_0^{T_0} r(t)\sum_{l=1}^{L_c} \tilde{\gamma}_l s(t-\tilde{\tau}_l)dt - \int_0^{T_0} \Big(\sum_{l=1}^{L_c} \tilde{\gamma}_l s(t-\tilde{\tau}_l)\Big)^2 dt \tag{2.20}$$

The second term of the right hand side of (2.20) can be written as

$$\begin{aligned} &\int_0^{T_0} \sum_{l=1}^{L_c} \tilde{\gamma}_l s(t-\tilde{\tau}_l) \sum_{m=1}^{L_c} \tilde{\gamma}_m s(t-\tilde{\tau}_m)dt \quad = \\ &\int_0^{T_0} \sum_{l=1}^{L_c}\sum_{m=1}^{L_c} \tilde{\gamma}_l\tilde{\gamma}_m s(t-\tilde{\tau}_l)s(t-\tilde{\tau}_m)dt \quad \overset{(a)}{=} \quad \begin{cases} 0, & \text{if } l \neq m \\ ME_b \sum_{l=1}^{L_c} \tilde{\gamma}_l^2, & \text{if } l = m \end{cases} \end{aligned} \tag{2.21}$$

where (a) holds because we assume that if $l \neq m$ the monocycles appearing in $s(t)$ are widely separated from each other and even a small time misalignment makes the echoes virtually orthogonal. Thus,

neglecting the correlation between signal echoes, we have for $l \neq m$ that

$$\int_0^{T_0} s(t-\tilde{\tau}_l)s(t-\tilde{\tau}_m)dt \approx 0 \tag{2.22}$$

Using (2.22), equation (2.21) can be written analytically as

$$\int_0^{T_0} \sum_{l=1}^{L_c}\sum_{m=1}^{L_c} \tilde{\gamma}_l\tilde{\gamma}_m s(t-\tilde{\tau}_l)s(t-\tilde{\tau}_m)dt = \int_0^{T_0} \sum_{l=1}^{L_c} \tilde{\gamma}_l^2 s^2(t-\tilde{\tau}_l)dt =$$
$$\sum_{l=1}^{L_c} \tilde{\gamma}_l^2 \int_0^{T_0} s^2(t-\tilde{\tau}_l)dt = \sum_{l=1}^{L_c} \tilde{\gamma}_l^2 M \int_0^{NT_f} s^2(t-\tilde{\tau}_l)dt = ME_b \sum_{l=1}^{L_c} \tilde{\gamma}_l^2$$

where E_b is the energy of $b(t)$

$$E_b = \int_0^{NT_f} b^2(t)dt \tag{2.23}$$

Then, performing some ordinary manipulations, we get

$$\log[\Lambda(\tilde{\boldsymbol{\gamma}}, \tilde{\boldsymbol{\tau}})] = 2\sum_{l=1}^{L_c} \tilde{\gamma}_l \int_0^{T_0} r(t)s(t-\tilde{\tau}_l)dt - ME_b \sum_{l=1}^{L_c} \tilde{\gamma}_l^2$$

or

$$\log[\Lambda(\tilde{\boldsymbol{\gamma}}, \tilde{\boldsymbol{\tau}})] = 2\sum_{l=1}^{L_c} \tilde{\gamma}_l \sum_{k=0}^{M-1} z_k(\tilde{\tau}_l, a_k) - ME_b \sum_{l=1}^{L_c} \tilde{\gamma}_l^2 \tag{2.24}$$

where $z_k(\tilde{\tau}_l, a_k)$ is response of the matched filter $b(-t)$ at $t = kNT_f + \Delta a_k + \tilde{\tau}_l$.

This can be explained as follows:

$$\begin{aligned}\int_0^{T_0} r(t)s(t-\tilde{\tau}_l)dt &= \int_0^{T_0} r(t)\sum_{k=0}^{M-1} b(t-kNT_f-a_k\Delta-\tilde{\tau}_l)dt \\ &= \sum_{k=0}^{M-1}\underbrace{\int_0^{T_0} r(t)b(t-kNT_f-a_k\Delta-\tilde{\tau}_l)dt}_{z_k(\tilde{\tau}_l,a_k)}\end{aligned}$$

But

$$r(t)\otimes b(-t)\Big|_{t=kNT_f+\Delta a_k+\tilde{\tau}_l} = \int_0^{T_0} r(\tau)b(\tau-t)d\tau\Big|_{t=kNT_f+\Delta a_k+\tilde{\tau}_l}$$

$$= \int_0^{T_0} r(\tau)b(\tau-kNT_f-\Delta a_k-\tilde{\tau}_l)d\tau$$

Using the above equations, we have

$$\begin{aligned}z_k(\tilde{\tau}_l,a_k) &= \int_0^{T_0} r(t)b(t-kNT_f-a_k\Delta-\tilde{\tau}_l)dt \\ &= [r(t)\otimes b(-t)]_{t=kNT_f+\Delta a_k+\tilde{\tau}_l} \qquad (2.25)\end{aligned}$$

where $\otimes$ denotes convolution operation.

From (2.24) it is seen that $\{z_k(\tilde{\tau}_l,a_k)\}$ are sufficient statistics to compute the ML estimates of $(\boldsymbol{\gamma},\boldsymbol{\tau})$, as it is seen in figure 2.2. The calculation of these statistics can be carried out as follows. Inserting (2.2) into (2.25) yields

$$z_k(\tilde{\tau}_l,a_k) = \sum_{j=0}^{N-1}[r(t)\otimes g(-t)]_{t=(kN+j)T_f+\Delta a_k+\tilde{\tau}_l+c_jT_c} \qquad (2.26)$$

which says that $z_k(\tilde{\tau}_l, a_k)$ is computed by feeding $r(t)$ to the filter matched to the monocycle and then sampling at the times $t_{k,j} = (kN + j)T_f + \Delta a_k + \tilde{\tau}_l + c_j T_c$, with $0 \leq j \leq N - 1$.

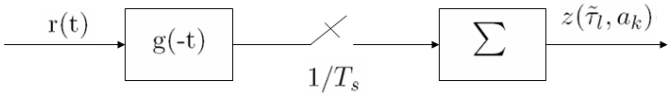

Figure 2.2: Computation of sufficient statistics.

Returning to (2.24), our task is to maximize $\log[\Lambda(\tilde{\boldsymbol{\gamma}}, \tilde{\boldsymbol{\tau}})]$ as a function of $\tilde{\boldsymbol{\gamma}}$ and $\tilde{\boldsymbol{\tau}}$. This can be done in two steps. First, we vary $\tilde{\boldsymbol{\gamma}}$ while keeping $\tilde{\boldsymbol{\tau}}$ fixed. If the maximum is found at $\hat{\boldsymbol{\gamma}}(\tilde{\boldsymbol{\tau}})$, then (second step) we replace $\tilde{\boldsymbol{\gamma}}$ with $\hat{\boldsymbol{\gamma}}(\tilde{\boldsymbol{\tau}})$ in $\log[\Lambda(\tilde{\boldsymbol{\gamma}}, \tilde{\boldsymbol{\tau}})]$ and look for the maximum of $\log[\Lambda(\hat{\boldsymbol{\gamma}}(\tilde{\boldsymbol{\tau}}), \tilde{\boldsymbol{\tau}})]$.

The first step is staightforward and yields from (2.24)

$$\frac{\partial \log[\Lambda(\tilde{\boldsymbol{\gamma}}, \tilde{\boldsymbol{\tau}})]}{\partial \tilde{\gamma}_l} = 0 \quad \Leftrightarrow \quad 2 \sum_{k=0}^{M-1} z_k(\tilde{\tau}_l, a_k) - 2ME_b\tilde{\gamma}_l = 0 \quad \Leftrightarrow$$

$$\tilde{\gamma}_l = \frac{1}{ME_b} J(\tilde{\tau}_l) \qquad 1 \leq l \leq L_c \tag{2.27}$$

with

$$J(\tilde{\tau}) = \sum_{k=0}^{M-1} z_k(\tilde{\tau}, a_k). \tag{2.28}$$

Next, substituting (2.27) into (2.24)

$$\begin{aligned}\log[\Lambda(\tilde{\boldsymbol{\gamma}},\tilde{\boldsymbol{\tau}})] &= 2\sum_{l=1}^{L_c}\frac{1}{ME_b}J^2(\tilde{\tau}_l) - ME_b\sum_{l=1}^{L_c}\frac{1}{M^2E_b^2}J^2(\tilde{\tau}_l)\\ &= \frac{2}{ME_b}\sum_{l=1}^{L_c}J^2(\tilde{\tau}_l) - \frac{1}{ME_b}\sum_{l=1}^{L_c}J^2(\tilde{\tau}_l)\\ &= \frac{1}{ME_b}\sum_{l=1}^{L_c}J^2(\tilde{\tau}_l) \qquad (2.29)\end{aligned}$$

and it turns out that the problem reduces to maximizing

$$\sum_{l=1}^{L_c}J^2(\tilde{\tau}_l). \qquad (2.30)$$

As the maximum of (2.30) is found by maximizing each term in the sum, our problem reduces to looking for the locations of the *extrema* of $|J(\tilde{\tau})|$. Once they are found, the path gains follow from (2.27) recalling that γ_l is a positive quantity

$$\tilde{\gamma}_l = \frac{1}{ME_b}|J(\tilde{\tau}_l)| \qquad 1 \le l \le L_c. \qquad (2.31)$$

Figure 2.3 illustrates a typical shape of $J(\tilde{\tau})/ME_b$ as obtained with a three-path channel and SNR $E_b/N_0 = 10$dB.

It is seen that three major positive peaks correspond to the signal echoes. However, the effect of noise and signal cross-correlation also

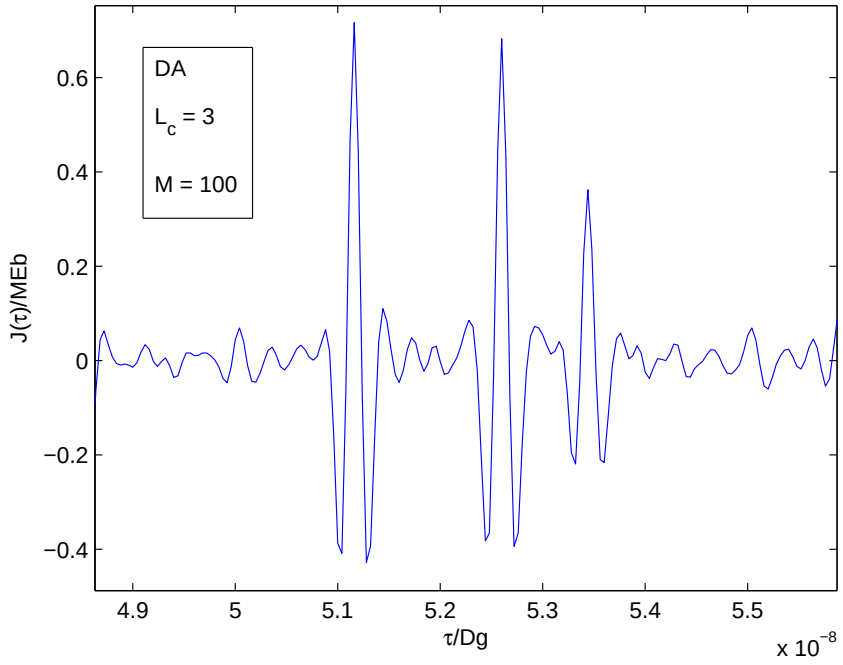

Figure 2.3: Typical shape of $J(\tilde{\tau})/ME_b$.

generates a number of other extrema (peaks). A first question is then: *which* peaks should we consider in a general situation? Stated in a different way, how can we distinguish signal echoes from artifacts of noise? From (2.31), we see that the largest peaks correspond to the strongest signal echoes. Thus, for high SNR values we expect that the L_c largest peaks are real echoes. On the other hand, since in practice we do not know the exact number of channel paths, *how many* peaks

should we take? A reasonable answer is that, since in a Rake-L receiver we can only exploit L paths, we should limit ourselves to the L largest peaks.

The extremely narrow pulses used for UWB transmission lead to inherent path diversity (i.e., independent fading of different multi path components). This implies that the received UWB signal contains a significant number of resolvable multi path components, which suggests a RAKE type receiver. This significantly reduces the fading effects and the resulting reduction of fading margins in link power budgets leads to reduced transmission power requirements.

Chapter 3

CHANNEL ESTIMATION AND FRAME SYNCHRONIZATION FOR UWB SIGNALS

3.1 Introduction

Time synchronization is a major challenge and a rich area of study in UWB communications systems. As with any other wireless commu-

nications system, time synchronization between the receiver and the transmitter is a must for UWB transmitter/receiver pairs. However, sampling and synchronizing nanosecond pulses place a major limitation on the design of the UWB systems. Moreover, the strict power limitations and short pulse duration make the performance of UWB systems highly sensitive to timing errors such as jitter and drift. This can become a major issue in the success of pulse-position-modulation (PPM) receivers, which rely on detecting the exact position of the received signal.

Whatever the receiver architecture, a synchronization circuit must provide accurate information on the arrival times of the incoming pulses. This is a critical issue that poses a serious challenge to the deployment of UWB radios as a viable and competitive wireless technology. Timing errors as small as fractions of a nanosecond can seriously degrade the system performance.

In UWB communications, a single data symbol is associated with several consecutive pulses, each located in its own frame. Multiple access to the channel is made possible by changing the pulse position within a

frame according to a user-specific time-hopping code. Timing recovery can be conveniently viewed as a process of estimating the beginning of the individual frames relative to the receiver's clock ticks. This is called *frame timing* (FT) [11].

3.2 Signal Format and Channel Model

The signal and channel model is similar to the previous one, but it is useful to introduce again some basic notations.

The transmitted signal is expressed as [8]

$$s(t) = \sum_{i} \sum_{j=0}^{N-1} g(t - iNT_f - jT_f - c_j T_c - a_i \Delta) \tag{3.1}$$

where (as in the previous chapter)

- $\{a_i\}$: information symbols taking values 0 or 1 with equal probability
- $g(t)$: monocycle
- N: number of frames per symbol
- T_f: frame period
- T_c: chip period
- Δ: PPM time shift
- $\{c_j\}_{j=0}^{N-1}$: time-hopping sequence

The channel model is quite general and takes into account propagation effects such as reflections, refractions and scattering from the objects within the medium. These effects are frequency-sensitive and produce path - dependent distortions on the received pulses. Thus, the channel response to a single pulse $g(t)$ takes the form

$$c(t) = \sum_{l=1}^{L_c} \gamma_l g(t - \tau_l) \tag{3.2}$$

where γ_l and τ_l are the gain and delay associated with the path, and L_c is the number of paths. The overall waveform resulting by the transmission of $s(t)$ may be written as

$$r(t) = \sum_{i} \sum_{j=0}^{N-1} \sum_{l=1}^{L_c} \gamma_l g(t - iNT_f - jT_f - c_j T_c - a_i \Delta - \tau_l) + w(t) \tag{3.3}$$

In this equation, $w(t)$ is white Gaussian noise and without loss of generality we assume that the minimum path delay $\tau_{min} = \min_l\{\tau_l\}$ is smaller than the frame duration T_f.

The received waveform is passed through a filter $g_R(t)$ and is sampled with period $T_s = T_f/Q$, which is a submultiple of T_f. The relationship between T_s and T_c is given by $T_c/T_s = 25$. Integer Q represents the

number of samples per frame. The filter output is

$$x(t) = \sum_{i} \sum_{j=0}^{N-1} \sum_{l=1}^{L_c} \gamma_l g_l(t - iNT_f - jT_f - c_j T_c - a_i \Delta - \tau_l) + n(t) \quad (3.4)$$

where $g_l(t)$ is the convolution $g(t) \otimes g_R(t)$ and $n(t)$ represents the filtered noise. This equation may be written in a more convenient form calling μ the integer part of τ_{min}/T_s and letting

$$\varepsilon_l = \tau_l - \mu T_s. \quad (3.5)$$

Note that μ takes values in the range $0 \leq \mu \leq Q - 1$ since $\tau_{min} < T_f$ by assumption. Substituting (3.5) into (3.4) and rearranging yields

$$x(t) = \sum_{i} \sum_{j=0}^{N-1} h(t - iNT_f - jT_f - c_j T_c - a_i \Delta - \mu T_s) + n(t) \quad (3.6)$$

with

$$h(t) = \sum_{l=1}^{L_c} \gamma_l g_l(t - \varepsilon_l). \quad (3.7)$$

Function $h(t)$ represents the channel response to a monocycle applied at $t = -\mu T_s$ and, in the sequel, is referred to as the channel response (CR). Note that the signal component in (3.6) corresponding to symbol a_k is

$$s_k(t) = \sum_{j=0}^{N-1} h(t - kNT_f - jT_f - c_j T_c - a_k \Delta - \mu T_s). \quad (3.8)$$

Thus, matched-filter detection requires knowledge of $h(t)$ and μ. Parameter μ indicates the frames' starting times (at $t = mT_f + \mu T_s$ with $m = 0, 1, 2, \ldots$).

In the following, we discuss an estimation strategy for $h(t), \mu$. Before proceeding, it is useful to remark on the channel estimation perspective we are taking here. It is clear from (3.6) that such a perspective subsumes any possible pulse distortion from the channel. In other words, we do not care about distortions because we look for the overall channel response rather than its individual components.

3.3 FT and Channel Estimation using LS techniques

In an indoor environment, each pulse generates hundreds of echoes, that can be resolved and combined in a Rake receiver to exploit the rich diversity of the multipath channel. With a pulse duration of 1 ns, it is shown that accurate timing is achieved with sampling rates of around 1 GHz. However, higher rates are needed to achieve satisfactory channel estimates.

We concentrate on a timing scheme based on least squares (LS) methods [11]. Essentially, we look for the minimum of the Euclidean distance between the received samples and a local replica of their noiseless components. To recover FT, a periodic pulse sequence with period T_f is used and the minimization produces a joint estimate of the channel response and the start of each frame. This algorithm is simple but it requires that the periodic sequence be transmitted by a single user at a time. Here again, we consider the scenario with a single user, so $\{c_j\} = 0$.

Assume that $h(t)$ is concentrated on the interval $[0, LT_s)$ and call $h[n] = h(nT_s)$ its samples at multiples of T_s. Letting

$$\mathbf{h} \triangleq [h[0], h[1], \ldots, h[L-1]]^T$$

be the sampled version of the CR, the estimation is carried out as follows. Parameters $\mathbf{h}$ and μ are estimated by transmitting a periodic signal of period T_f [this corresponds to setting $a_{i(=0)} \equiv 1$ in (3.1)]. We assume that there is no interframe interference, meaning that the channel responses from different monocycles are not overlapped. This requires that T_f exceeds the channel delay spread LT_s plus the maximum difference between consecutive time shifts of the hopping code. Such an assumption greatly simplifies the analysis and allows us to focus on the fundamental aspects of the UWB signal acquisition.

The received waveform in the first phase is

$$x(t) = \sum_{j=0}^{N-1} h(t - jT_f - \Delta - \mu T_s) + n(t). \tag{3.9}$$

In a given frame, the summation in (3.9) consists of two parts: the truncated CR originating in the current frame and the tail of the CR from the previous frame. Figure 3.1 illustrates the periodic nature of

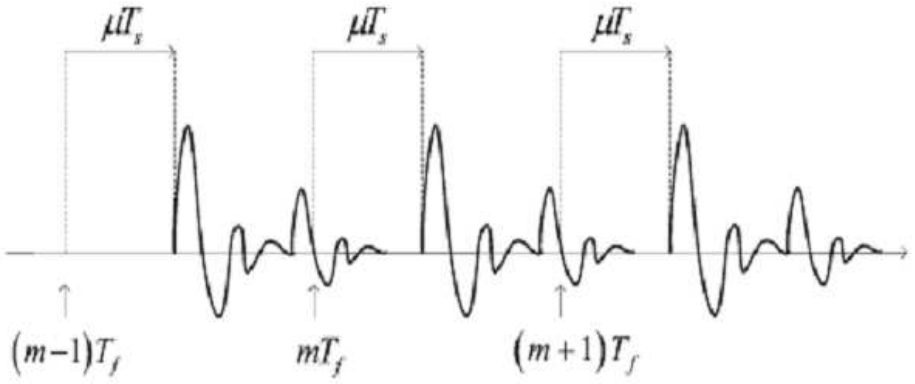

Figure 3.1: Noise - free component of the received waveform with no modulation.

the noise - free component of $x(t)$. The latter is the missing part of the former and vanishes if $T_f - \mu T_s$ exceeds LT_s. Now, suppose that $x(t)$ is observed over M_f' frames and is sampled at $t = mT_f + nT_s$, with $m = 0, 1, \ldots, M_f' - 1$ and $n = 0, 1, \ldots, Q - 1$. Letting

$$x_m[n] \stackrel{\Delta}{=} x(mT_f + nT_s)$$

and collecting the samples from the mth frame into

$$\mathbf{x}_m \stackrel{\Delta}{=} [x_m[0], x_m[1], \ldots, x_m[Q-1]]^T$$

the noise-free components of $\mathbf{x}_m$ may be represented as follows.

Denote $\mathbf{p}$ the Q-dimensional vector obtained by extending $\mathbf{h}$ with $Q-L$ zeroes

$$\mathbf{p} \triangleq [h[0], h[1], \ldots, h[L-1], \underbrace{0, 0, \ldots, 0}_{Q-L}]^T \tag{3.10}$$

and call $\mathbf{v}^{(\downarrow)}[\mu, \mathbf{h}]$ the vector resulting from downshifting the components of $\mathbf{p}$ by μ steps and zero-padding the empty places

$$\mathbf{v}^{(\downarrow)}[\mu, \mathbf{h}] \triangleq [\underbrace{0, 0, \ldots, 0}_{\mu}, h[0], h[1], \ldots, h[Q-\mu-1]]^T. \tag{3.11}$$

It is easily seen that $\mathbf{v}^{(\downarrow)}[\mu, \mathbf{h}]$ represents the (truncated) response originated in the mth frame. Similarly, let $\mathbf{v}^{(\uparrow)}[\mu, \mathbf{h}]$ be the Q-dimensional vector resulting by up-shifting the components of $\mathbf{p}$ by μ steps and zero-padding the empty places

$$\mathbf{v}^{(\uparrow)}[\mu, \mathbf{h}] \triangleq [h[\mu], h[\mu+1], \ldots, h[L-1], \underbrace{0, 0, \ldots, 0}_{Q-L+\mu}]^T. \tag{3.12}$$

Clearly, $\mathbf{v}^{(\uparrow)}[Q-\mu, \mathbf{h}]$ represents the tail of the response from the previous frame. Collecting these facts together, we have

$$\mathbf{x}_m = \mathbf{v}^{(\downarrow)}[\mu, \mathbf{h}] + \mathbf{v}^{(\uparrow)}[Q-\mu, \mathbf{h}] + \mathbf{n}_m \tag{3.13}$$

where $\mathbf{n}_m$ accounts for the noise.

The joint estimation of $\mathbf{h}$ and μ is performed with LS techniques as follows. We seek the values $\tilde{\mu}$ and $\tilde{\mathbf{h}} = [\tilde{h}[0], \tilde{h}[1], \ldots, \tilde{h}[L-1]]$ that minimize the squared Euclidean distance

$$D^2(\tilde{\mu}, \tilde{\mathbf{h}}) = \sum_{m=0}^{M_f'-1} \left\| \mathbf{x}_m - \mathbf{v}^{(\downarrow)}[\tilde{\mu}, \tilde{\mathbf{h}}] - \mathbf{v}^{(\uparrow)}[Q - \tilde{\mu}, \tilde{\mathbf{h}}] \right\|^2. \tag{3.14}$$

Substituting (3.11) and (3.12) into (3.14) yields

$$D^2(\tilde{\mu}, \tilde{\mathbf{h}}) = \sum_{m=0}^{M_f'-1} \sum_{l=0}^{L-1} \Big(x_m[|l+\tilde{\mu}|_Q] - \tilde{h}[l] \Big)^2 + \sum_{m=0}^{M_f'-1} \sum_{l=L}^{Q-1} \Big(x_m[|l+\tilde{\mu}|_Q] \Big)^2 \tag{3.15}$$

where $|l + \tilde{\mu}|_Q$ means $(l + \tilde{\mu})$ mod$-Q$. Alternatively, (3.15) may be written as

$$D^2(\tilde{\mu}, \tilde{\mathbf{h}}) = \sum_{m=0}^{M_f'-1} \sum_{l=0}^{Q-1} \Big(x_m[|l+\tilde{\mu}|_Q] \Big)^2 + M_f' \sum_{l=0}^{L-1} \Big(\tilde{h}[l] \Big)^2 - 2 \sum_{m=0}^{M_f'-1} \sum_{l=0}^{L-1} \tilde{h}[l] x_m[|l+\tilde{\mu}|_Q]. \tag{3.16}$$

Differentiating with respect to the $\tilde{h}[l]$'s, setting the result equal to zero and solving for $\tilde{h}[l]$ yields

$$\frac{\partial}{\partial \tilde{h}[l]} \Big(D^2(\tilde{\mu}, \tilde{\mathbf{h}}) \Big) = 0 \quad \Leftrightarrow$$

$$2M_f' \sum_{l=0}^{L-1} \tilde{h}[l] - 2 \sum_{m=0}^{M_f'-1} \sum_{l=0}^{L-1} x_m[|l + \tilde{\mu}|_Q] = 0$$

or finally

$$\tilde{h}[l] = \frac{1}{M_f'} \sum_{m=0}^{M_f'-1} x_m[|l+\tilde{\mu}|_Q], \quad 0 \le l \le L-1. \tag{3.17}$$

Next, substituting (3.17) into (3.16) produces

$$D^2(\tilde{\mu}, \tilde{\mathbf{h}}) = \sum_{m=0}^{M_f'-1} \sum_{l=0}^{Q-1} \Big(x_m[|l+\tilde{\mu}|_Q] \Big)^2 - \frac{1}{M_f'} \sum_{l=0}^{L-1} \left(\sum_{m=0}^{M_f'-1} x_m[|l+\tilde{\mu}|_Q] \right). \tag{3.18}$$

On the other hand, as there are Q samples in a frame, we have

$$\sum_{l=0}^{Q-1} \Big(x_m[|l+\tilde{\mu}|_Q] \Big)^2 = \sum_{l=0}^{Q-1} (x_m[l])^2 \tag{3.19}$$

which shows that the first term in (3.18) is independent of $\tilde{\mu}$. Thus, minimizing $D^2(\tilde{\mu}, \tilde{\mathbf{h}})$ amounts to maximizing the second term, i.e.,

$$\hat{\mu} = \arg \max_{0 \le \tilde{\mu} \le Q-1} \left\{ \sum_{l=0}^{L-1} \left(\sum_{m=0}^{M_f'-1} x_m[|l+\tilde{\mu}|_Q] \right)^2 \right\}. \tag{3.20}$$

Finally, setting $\tilde{\mu} = \hat{\mu}$ in (3.17) yields the CR estimate

$$\hat{h}[l] = \frac{1}{M_f'} \sum_{m=0}^{M_f'-1} x_m[|l+\hat{\mu}|_Q], \quad 0 \le l \le L-1. \tag{3.21}$$

With this algorithm, the tracking is implemented by repeating the estimation procedure at regular intervals. In doing so, a reduction in the data rate is incurred as no information is transmitted during the synchronization intervals.

Chapter 4

SIMULATION RESULTS

4.1 Performance Evaluation

The performance evaluation of the previous data-aided estimation and the FT synchronization has been assessed by simulation. With reference to (2.1) and (2.2), the following assumptions have been made. We have chosen the monocycle shape as the second derivative of a Gaussian function

$$g(t) = \left[1 - 4\pi\left(\frac{t - D_g/2}{D_g}\right)^2\right] \exp\left[-2\pi\left(\frac{t - D_g/2}{D_g}\right)^2\right]. \quad (4.1)$$

The monocycle duration D_g is taken as a time unit in the simulations. Time parameters in (2.1) and (2.2) are related to D_g by $\Delta = D_g$, $T_f = 40D_g$, and $T_c = T_f/20$. Note that a comparatively small duty cycle T_f/D_g of 40 is adopted to keep the simulation time within acceptable limits.

An idea of the estimation accuracy of the DA algorithm is gathered from the following experiment in which three-path channels ($L_c = 3$) are assumed. The desired user's channel has fixed path gains ($\gamma_1 = 0.73, \gamma_2 = 0.67, \gamma_3 = 0.35$) and delays ($\tau_1 = 30ns, \tau_2 = 66ns, \tau_3 = 87ns$).

BER performance has been assessed with Rake-3 and Rake-1. The problem is to approximate the actual channel with a channel with L_c branches and to choose the propagation parameters in the latter in such a way that its output matches the recorded waveform as best as possible. Clearly, the degree of matching depends on L_c and the minimum value of L_c required for a good match establishes the number of fingers that a Rake receiver must possess to efficiently exploit the channel diversity. Rake-1 is simpler than Rake-3, but has poorer performance as

it exploits a smaller fraction of the available signal energy.

The performance of the estimation algorithms is expressed as a function of the SNR. The former is defined as the ratio E_b/N_0, where E_b is the energy of the noiseless channel output.

In the first algorithm we have used 50 symbols per packet (10 training symbols and 40 data symbols) and in the second one 50 data symbols. The difference is that in the second algorithm the data transmission is interrupted at regular intervals and replaced by a periodic signal at frame rate. In both methods the samples per packet is $Q = 800$.

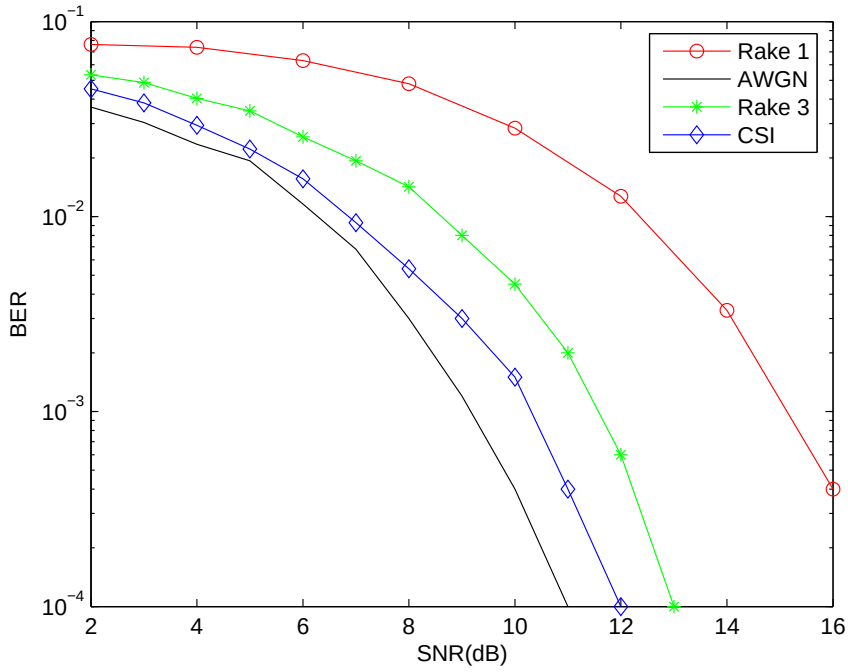

Figure 4.1: BER curves with DA estimation and CSI

Figure 4.1 illustrates the BER performance in DA estimation case and in ideal channel state information (CSI), meaning that the desired user's parameters are perfectly known. The bottom line represents the receiver performance over a Gaussian channel. It is clear from the figure that a Rake receiver with 3 fingers has better performance than the one with one finger, as it is expected.

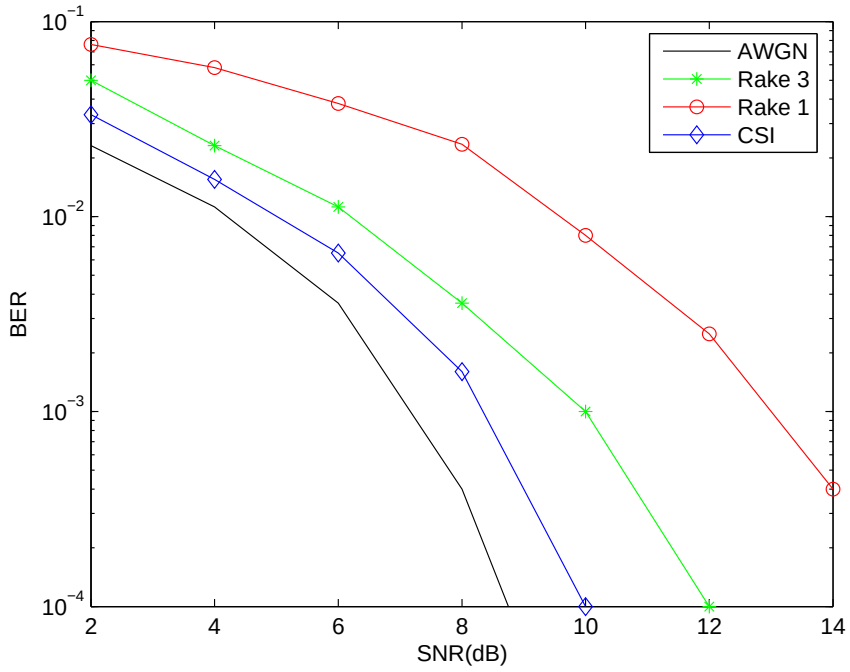

Figure 4.2: BER curves with second method (synchronization-estimation)

Figure 4.2 depicts the BER performance of a correlation receiver, where the parameters $\mu, \mathbf{h}$ are estimated. Again, Rake-3 receiver is better. In both algorithms, degradations with respect to CSI depend on the number of Rake fingers and the estimation method.

Chapter 5

CONCLUSION

In this thesis, we described a channel parameter estimation for UWB systems in a multipath environment [9]. The DA estimation technique is based on the ML criterion. We have also described another algorithm for channel estimation and frame synchronization [11]. Both operate on samples of the received waveform taken at high rate on the order of GHz.

Simulations have been run to assess the BER performance of correlation receivers with both algorithms. Their performances are almost the same. Moreover, their performance worsens as the sampling rate

decreases as a consequence of the reduced signal energy in the samples. Due to its significant bandwidth, a UWB-based radio communication system can accommodate many users. Usually, it is preferred to conceive of multiple access with UWB signals as being accomplished with code-division multiplexing (CDM) in conjunction with pulse-position modulation (PPM), because code correlation is a useful method for isolating multipaths. In order to eliminate catastrophic collisions due to multiple access, each user j is assigned a time-shift pattern c_j, as mentioned before, called a time-hopping sequence (TH-UWB). With TH, each pulse is positioned within each frame duration T_f according to a user-specific TH sequence. Specifically, dividing each frame into N_c chips each of duration T_c, the jth user's TH code c_j corresponds to a time shift of $c_j T_c$ during the nth frame. In other words, multiple access is achieved by altering the pulse *position* from frame to frame, according to the sequence c_j. Depending on the spreading codes employed, the UWB systems are termed TH-UWB, direct sequence (DS)-UWB, or baseband single-carrier/multicarrier (SC-MC)-UWB.

Bibliography

[1] http://www.intel.com/technology/comms/uwb/download/W241Paper.pdf

[2] Jeffrey H. Reed, "*An Introduction to Ultra Wideband Communication Systems,*" Prentice-Hall, 2005.

[3] http://www.antd.nist.gov/wctg/manet/NISTUWBReportApril03.pdf

[4] http://www.fcc.gov/oet/info/rules/part15/part15-8-14-06.pdf

[5] A. F. Molisch "*Ultawideband Propagation Channels-Theory, Measurement, and Modeling,*" IEEE Transactions on Vehicular Technology, vol. 54, no. 5, pp. 1528-1545, September 2005.

[6] L. Yang and G. B. Giannakis "*Ultra-Wideband Communications An Idea Whose Time Has Come,*" IEEE Signal Proccessing Magazine, November 2004.

[7] V. Lottici, A. D'Andrea and U. Mengali "*Channel Estimation for Ultra-Wideband Communications,*" IEEE Journal on Selected Areas in Communications, vol. 20, no. 9, pp. 1638-1645, December 2002.

[8] M. Z. Win and R. A. Scholtz, "*Impulse Radio: How It Works,*" IEEE Communications Letters, vol. 2, no. 2, pp. 36-38, February 1998.

[9] Umberto Mengali and Aldo N. D'Andrea, "*Synchronization Techniques for Digital Receivers,*" Plenum Press, 1997.

[10] H.L.Van Trees "*Detection, Estimation, and Modulation: Part I,*" New York: Willey, 1968.

[11] C. Carbonelli and U. Mengali "*Synchronization Algorithms for UWB Signals,*" IEEE Transactions on Communications, vol. 54, no. 2, pp. 329-338, February 2006.